Jurnal Teknologi, 42(D) Jun. 2005: 113–132

AREA-BASED CONCENTRATION MEASUREMENT USING OPTICAL TOMOGRAPHY TECHNIQUE FOR VARIOUS FLOW PATTERNS

RUZAIRI ABDUL RAHIM,[1]* PANG JON FEA,[2] CHAN KOK SAN,[3] & LEONG LAI CHEAN[4]

Abstract. The common application for process tomography is to visualize cross-sectional images of multi-phase flow system such as solid/gas, gas/liquid and water/oil. The flow pattern of the flow system will directly influence the concentration measurement. The main purpose of this paper is to investigate various flow patterns using optical tomography. The optical tomography sensor in the measurement system is constructed by using four parallel beam projections using infrared light source in 85 mm inner diameter pipeline. Sensor modeling and reconstruction algorithm are discussed. The measurement results are analyzed and conclusion is made to note which kind of flow pattern is suitable to be measured by optical tomography.

Abstrak. Applikasi proses tomografi secara am adalah untuk melihat kepekatan susuk sesebuah aliran berbagai fasa. Bentuk sesebuah aliran mempengaruhi keputusan kepekatan susuk yang dihasilkan. Tujuan utama kertas kerja ini adalah untuk menyelidik kesan bentuk aliran ke atas proses tomografi jenis optik. Tomografi optik dibentuk dengan menggunakan empat unjuran secara selari. Punca cahaya adalah LED dan saiz paip adalah 85 mm. Pemodelan penderia dan pembinaan semula imej juga dibincangkan. Keputusan pengukuran dianalisa untuk menunjukkan bentuk aliran yang sesuai untuk proses tomografi optik.

1.0 INTRODUCTION

Process tomography involves the acquisition of measurement signals from sensors located at the periphery of an object [1]. It provides an increase in the quantity and quality of information when compared to many earlier measurement techniques [2]. The parameter or characteristic to be imaged is determined by the type of sensor chosen. In this regard, gamma-rays and X-rays are sensitive to density, whereas capacitance sensors are sensitive to the dielectric constant of the object. To construct cross-sectional image, the sensor signals are amplified, filtered, digitized and finally processed in a computer using an image reconstruction algorithm. Normally, most of

[1,2,3&4] Process Tomography Research Group (PROTOM), Control & Instrumentation Engineering Department, Faculty of Electrical Engineering, Universiti Teknologi Malaysia, 81310 Skudai, Johor Bahru, Malaysia.
*Corresponding author: Email: ruzairi@.fke.utm.my, ruzairiabdulrahim@yahoo.co.uk

the flow information is from the concentration measurement. For example, the cross-sectional image itself already provides material flow concentration. On the other hand, hundreds of upstream and downstream images can provide flow velocity when correlation function is correctly applied.

In the field of optical tomography, cross-sectional image reconstruction is based on sensor arrangement and image reconstruction algorithm. Most of the existing cross-sectional images using different types of optical tomography sensors suffer from the problem of obtaining wrong image, called the ambiguous or blurred image. This project applies as hybrid image reconstruction algorithm [3] to reduce the ambiguity. Various flow patterns were investigated so that their influence on the concentration measurement can be realized.

2.0 SENSOR PROJECTION GEOMETRY

There are many types of projection patterns that can be used to detect the flow materials within pipeline in optical tomography. Basically, they can be divided into groups of parallel beam projections and fan beam projections as shown in Figure 1.

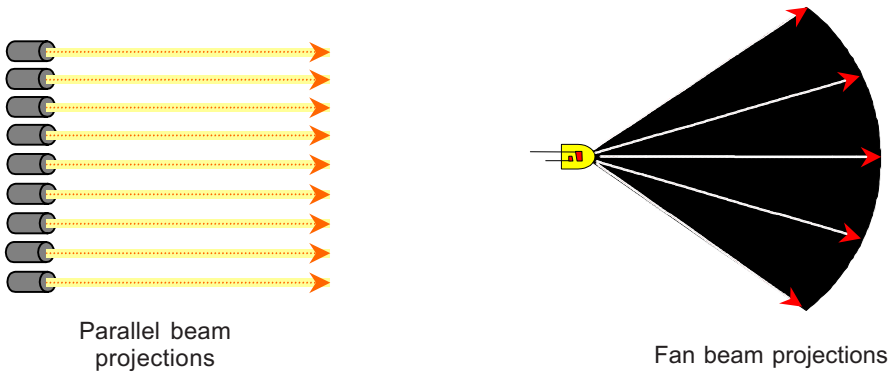

Figure 1 The parallel beam and fan beam projections

The parallel beam projection can be obtained through the arrangement of several transmitter sensors in a straight line and the view angle of each sensor is considered small. This type of projection results in patterns of two orthogonal projections, two rectilinear projections, combination of one orthogonal with two rectilinear projections and combination of two orthogonal with two rectilinear projections [4]. This paper adopts the last projection pattern because it can provide sufficient information to prevent as much as possible ambiguous effect from arising during cross-sectional image detection compared to the previous three projections.

The two orthogonal and two rectilinear projections are shown in Figures 2 (a) and 2 (b). In the two orthogonal projections, there are two arrays of projections. One is

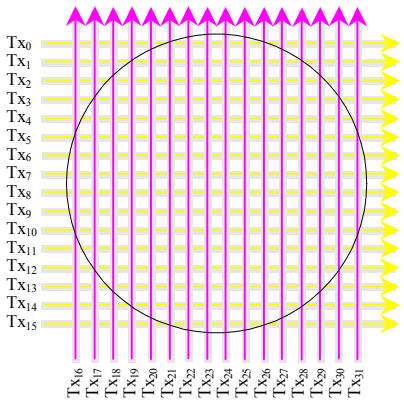

(a) Two orthogonal projections

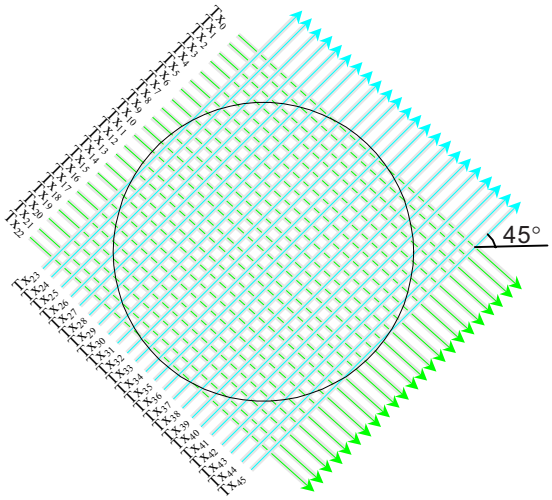

(b) Two rectilinear projections

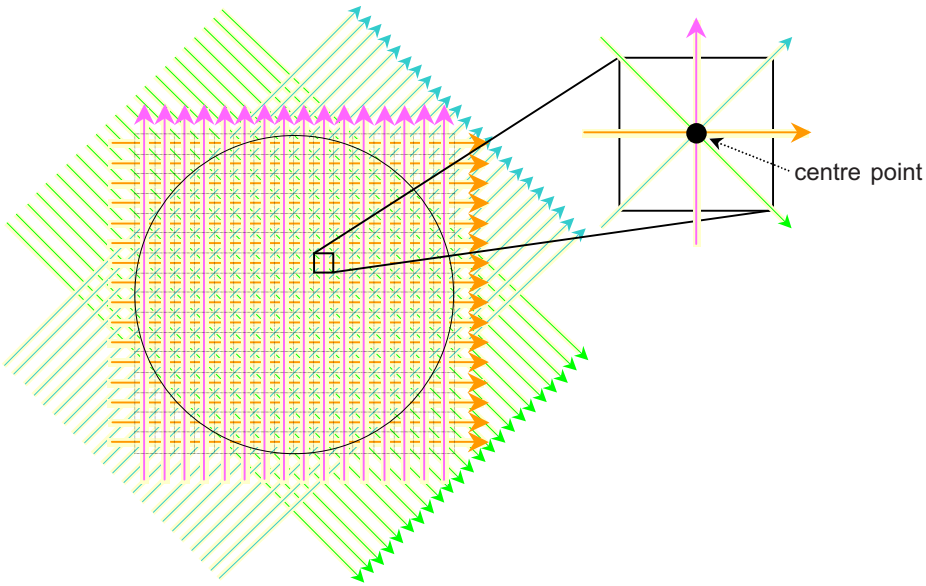

(c) Combination of two orthogonal and two rectilinear projections

Figure 2 Projection geometry for this project

parallel to the horizontal axis while the other is parallel to the vertical axis. In this paper, an array of projections uses 16 pairs of transmitter-receiver and this resulted in an image resolution of 16×16 pixels. For the two rectilinear projections, both arrays of projections are inclined plus and minus 45° to the horizontal axis respectively. The

number of transmitter-receiver pairs used in one array is 23 because each emitter projection in this layer must cross over the centre point of the corresponding pixel and also the area within the pipeline as shown in Figure 2 (c). In [3], the same projection geometry using 8×8 pairs of transmitter-receiver for the two orthogonal projections and 11×11 pairs of transmitter-receiver for the two rectilinear projections.

3.0 SENSOR MODELING

Modeling in process tomography is mostly used to predict the sensor output voltage. The forward problem is modelled to solve the inverse problem for obtaining image. In the previous research reported [2], the optical path length model was used to predict the amplitude of sensor output voltage and he successfully related it to the various mass flow rates of sand flow. In [3], both models of optical path length and optical attenuation were investigated to explore how two different parameters affected the measured output voltage of the tomography sensor in the measurement of gas bubbles in vertical water. The optical path length is referred as the projection's sensing beam within pipeline whereas optical attenuation is referred as the change in optical density within the pipeline according to Lambert Beers Law.

This project applies path width model because the signal conditioning system that employs light intensity measurement is not suitable for optical path length model [5]. Solid materials as flowing objects that have high absorptions characteristic is not suitable to use optical attenuation model because this kind of model must assume both conveyed and conveying mediums are transparent [3]. This model was applied in the previous research done in [5] using fan beam projections. Although there are two layers of projections in the sensor design, only the sensors output voltage of two orthogonal projections layer are used to construct the concentration image. The sensors output voltages of two rectilinear projections are only used to verify the location of flow materials. Therefore, the modelling concentrates on the two orthogonal projections layer.

The principle of the modelling is based on the light beams transmitting in straight line to receivers. The sensor output voltage depends on the blockage effect when objects intercept the light beams. There are two assumptions in this model. First, all incident lights on the surface of object are fully absorbed by the object [5]. Second, light scattering and beam divergence effect are neglected [2].

The forward problem for this model generates a series of sensitivity map and each map is associated with a specific sensor. The size of sensitivity map is obtained from the two orthogonal projections layer, which is 16×16 pixels. For each sensitivity map, it contains values of '1' and '0'. It is because all pixels in the map are constructed by drawing 17 vertical lines intercepting with 17 horizontal lines and each sensor projection beam is also parallel to the direction of those lines depending on the sensor location. The beam's area that cross over each pixel is identical as shown in Figure 3 (a). In fan

beam projection using one emitter and several receivers, the beam's area that cross over each pixel depends on the position of receivers placed around the pipe as illustrated in Figure 3 (b). Therefore, the sensitivity map in this case consists of various values depending on the mathematical modelling. To generate the sensitivity map of sensor S_3 that is represented in Figure 4, the pixels being crossed by the projection beam are filled with '1' and the other pixels are filled with '0'. This case is only true within the pipeline area. Those pixels outside the pipeline (represented by a circle) will be assigned value '0'.

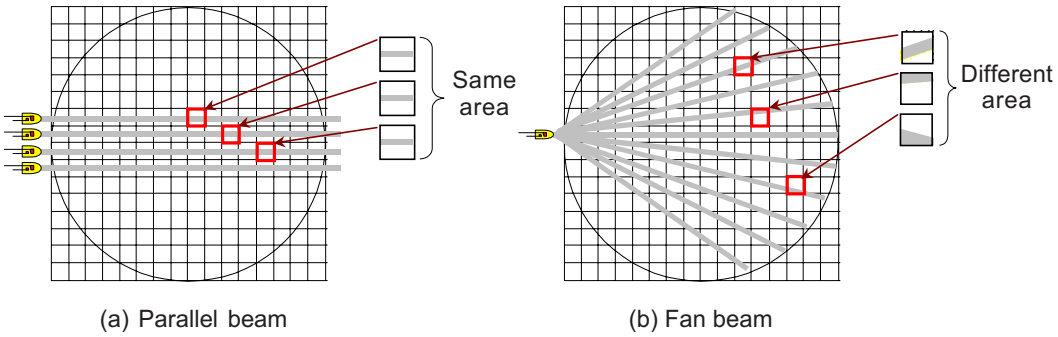

Figure 3 Projection beam cross over the pixels of sensitivity map

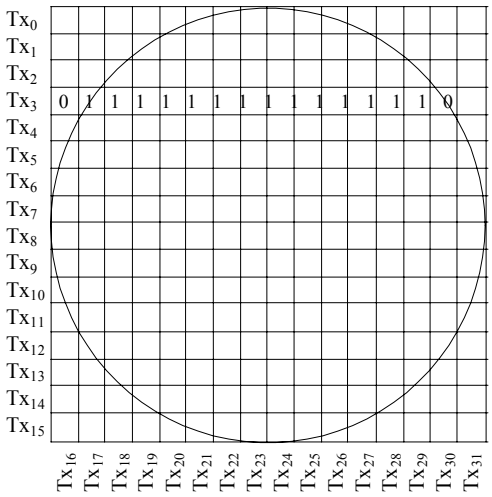

Figure 4 Sensitivity map of sensor

Since the two orthogonal projections layer consist of 32 pairs of emitter-receiver sensors, the optical path width model is able to predict all 32 receivers output voltage based on the following equation,

$$V_{Si} = \begin{cases} \dfrac{w(x_i, y_L)}{w_{FH}} \times V_m & ; \quad 0 \le i \le 15 \\ \dfrac{w(x_L, y_i)}{w_{FV}} \times V_m & ; \quad 0 \le i \le 15 \end{cases} \tag{1}$$

where V_{Si} is sensor output voltage, $w(x_i, y_L)$ is the object's width referring to the horizontal axis, x_i is coordinate x corresponding to sensor i, y_L is coordinate y corresponding to sensor i which the maximum width blocked by an object, w_{FH} is the pixel's width referring to the horizontal axis, V_m is the maximum voltage that the receiver can obtain $(5V)$, $w(x_L, y_i)$ is the object's width referring to the vertical axis, x_L is coordinate y corresponding to sensor i that consist maximum width blocked by an object, y_i is coordinate y corresponding to sensor i and w_{FV} is pixel's width referring to the vertical axis. The maximum output voltage detected by the receiver will be 5 volt based on the signal conditioning circuit design.

4.0 IMAGE RECONSTRUCTION ALGORITHM

A tomography system must have the image reconstruction algorithm to compute cross-sectional image. Most of the image reconstruction algorithms applied in industry tomography come directly from medical tomography. Among them, back projection algorithm can be said to be the favourite among most of the researchers and resulting in many variations, such as linear back projection, filtered back projection, convolution back projection and graphical back projection. The other algorithms of image reconstruction include the hybrid reconstruction algorithm and algebraic reconstruction techniques (ART).

4.1 Linear Back Projection Algorithm (LBP)

Linear back projection is known as layergram back projection. The concept of this algorithm can be simply explained by referring to two orthogonal projections sensor. Consider an object inside the pipeline will block the light transmitted from the emitter to receiver (voltage of receiver increases when blocking is detected) as shown in Figure 5 (a). Then, receiver value will be filled into the pixels that linear to it like back projects something to the emitter as shown in Figure 5 (b). Each pixel will sum all corresponding receiver values to produce the concentration profile [5]. The highest pixel value shows the location of the object. However, this reconstruction algorithm will result in blurry or ambiguous image.

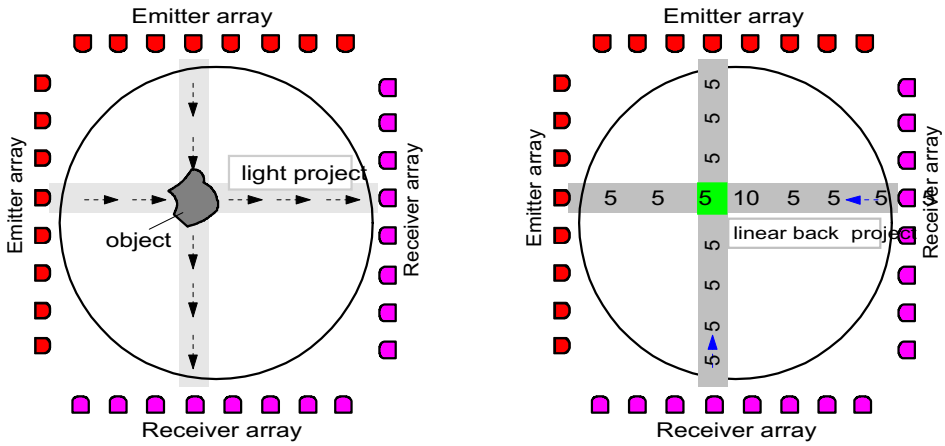

Figure 5 (a) Light projection and (b) Image reconstruction

4.2 Filtered Back Projection Algorithm (FBP)

This algorithm is widely used in most circumstances either in medical tomography or in industrial tomography because it can reconstruct better image compared to LBP algorithm. The concept of using this algorithm is applying a filter to the image reconstructed by LBP. The filter can reduce low frequency information and enhance high frequency information, sharpening edges, and reducing blurs. There are many versions of this algorithm. One of them is creating a filtered mask using full flow model. The filter is formed by calculating the ratio of maximum value allowed in concentration matrix to each element in the full flow concentration matrix [5]. Another version is using filters like the hamming filter, ramp filter, low pass filter and so on.

4.3 Convolution Back Projection Algorithm (CBP)

This algorithm is the most widely used method of reconstruction used by commercial computed tomography scanners (Xie, 1995). The popularity of CBP is caused by the procedure of reconstruction that does not require the filtering after the back projection [5]. The concept of using this algorithm can be understood by following the three steps below:

(i) Measure projections data
(ii) Filter projections data
(iii) Back project the filtered projections data

4.4 Graphical Back Projection Algorithm (GBP)

This algorithm is developed by Chan [5] for 16 fan beam projections. It is performed by utilizing the computer's graphical memory. The sensitivity map for each view in projections is not required during the reconstruction of image. To use this algorithm, a computer memory area with the size equivalent to $n \times n$, whereby n is the resolution of reconstructed image is declared as Device Independent Bitmap (DIB). The positions of 128 nodes in $n \times n$ map (Cartesian coordinate) are pre-calculated and stored in the computer's memory. The obtained data are stepped down into 8 bits digitalized value. A look-up table with 256 members is used to store a range of gradient colour values from 0 (white) to 255 (dark). To reconstruct the image, the 16 polygon shapes of light beams in each projection are drawn into the DIB (same as back projecting the light) using the corresponding nodes for each light beam and also filling the polygons with colour predetermined in look-up table that match the view's data [5].

The disadvantage of this algorithm is its limitation to be implemented in powerful high level programming language only. The software like Matlab, LabView and Lab Windows are unable to program this algorithm.

4.5 Hybrid Reconstruction Algorithm

This algorithm is proposed by [3]. The main purpose of it is to improve the accuracy of the image reconstruction using LBP by neglecting the blurry image. The algorithm assumes binary values from the sensor, either zero for no material or one for the presence of material [3]. The sensor value is first measured, if the reading is zero, then any pixels traversed by that sensor's beam are set to zero and omitted from further calculations. Only the rest of the pixels will perform LBP as usual.

4.6 Algebraic Reconstruction Technique (ART)

ART is one of a variety of iterative reconstruction algorithm in which the computed projections or ray sums of an estimated image are compared with the original projection measurement and the resulting errors are applied to correct the estimated image. The correction can be made using ray-by-ray correction technique, whereby the error is computed and the image is updated for a single ray-sum before proceeding to next ray-sum.

ART has a number of advantages, such as it can be used for any scanning geometry, incomplete data problem and if the projections are not uniformly distributed. Nevertheless, it is worth mentioning that ART is usually more time consuming than CBP algorithm.

Although there are many image reconstruction algorithms available that can be applied into industrial process tomography, only the Hybrid image reconstruction algorithm is used in this project because it can directly prevent ambiguous effect or

smearing effect and easy to apply. The ambiguous effect means that the reconstructed image contains certain wrong parts of the image showing objects are being detected, but in reality nothing appears at the areas mentioned. There are 3 factors resulting in this effect. First, the image reconstruction algorithm used is unable to prevent this effect. Second, in parallel beam projection, fewer number of projections arrays (e.g. 2 projections arrays) will result in insufficient information to verify the location of the objects. Normally, 4 and above projections arrays can provide adequate information to detect the objects' location and this is why this project uses 4 projections arrays in the geometry of two orthogonal and two rectilinear. The last factor is the shape of the object. The object's boundary that contains 'V' shape, such as star and three quarter circle will result in ambiguous effect. Optical tomography is unable to detect these kinds of objects because the space within the 'V' shape will be detected as a part of the object as shown in Figure 6.

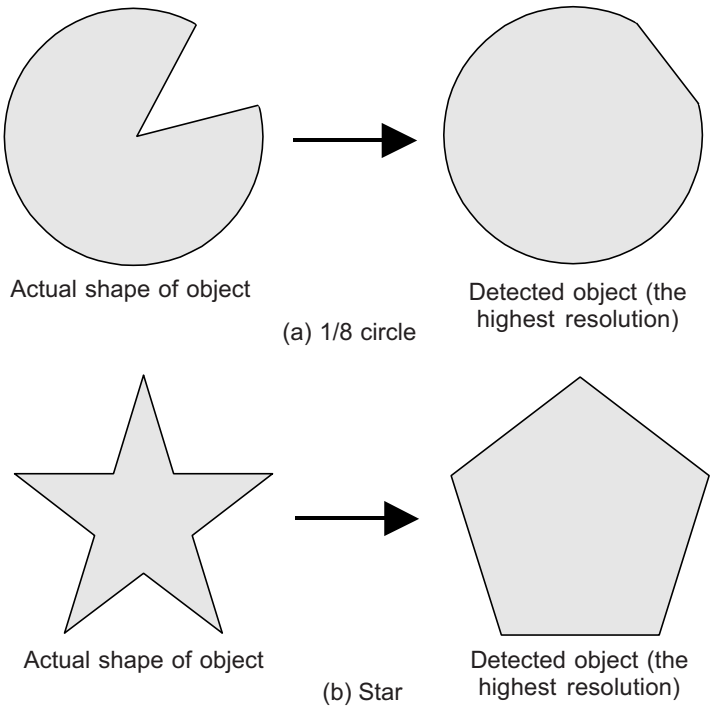

Figure 6 Ambiguous effect caused by object's shape using optical tomography

The hybrid image reconstruction described as the combination of the Linear Back Projection (LBP) algorithm with several masking conditions. Figure 7 depicts the application of the LBP algorithm.

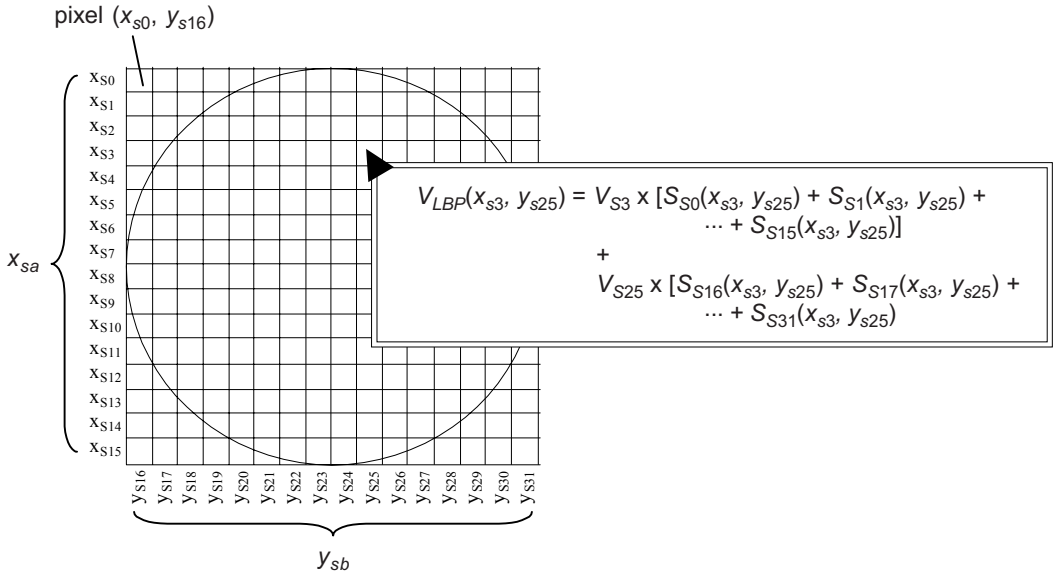

Figure 7 LBP algorithm for pixel (x_{s3}, y_{s25})

To obtain the concentration profile of 16×16 pixels, the following equation is used,

$$V_{LBP}(x_{sa}, y_{sb}) = V_{sa} \sum_{p=0}^{15} S_{Sp}(x_{sa}, y_{sb}) + V_{sb} \sum_{q=16}^{31} S_{Sp}(x_{sa}, y_{sb}) \quad (2)$$

where $V_{LBP}(x_{sa}, y_{sb})$ is a voltage of pixel (x_{sa}, y_{sb}) inside the concentration profile that uses LBP algorithm, x_{sa} is the coordinate x corresponding to sensor $S_0 - S_{15}$, y_{sb} is the coordinate y corresponding to sensor $S_{16} - S_{31}$, V_{Sa} is the sensor S_a output voltage ($0 \le a \le 15$), $S_{Sp}(x_{sa}, y_{sb})$ is pixel (x_{sa}, y_{sb}) in the sensitivity map of sensor S_p, V_{Sb} is sensor S_b output voltage ($16 \le b \le 31$) and $S_{Sq}(x_{sa}, y_{sb})$ is pixel (x_{sa}, y_{sb}) in the sensitivity map of sensor S_q.

Since the maximum sensor output voltage of V_{sa} and V_{sb} is 5 volt and the sensitivity map contains values '1' and '0' only, the maximum voltage of each pixel in the concentration profile can achieve 10 volt. By using a colour bar that is proportional to the voltage in the range of 0 – 10 volt, the concentration profile can be converted into image. Referring to Equation (2), notice that the answer of $\sum_{p=0}^{15} S_{Sp}(x_{sa}, y_{sb})$ and $\sum_{q=16}^{31} S_{Sq}(x_{sa}, y_{sb})$ for all pixels within pipeline is '1'. Hence, the equation can be simplified as follows,

$$V_{LBP}(x_{sa}, y_{sb}) = \begin{cases} V_{sa} + V_{sb} & ; \quad (x_{sa}, y_{sb}) \text{ inside pipeline} \\ 0 & ; \quad (x_{sa}, y_{sb}) \text{ outside pipeline} \end{cases} \tag{3}$$

Practically, sensor output voltage during no flow is not zero. So, the threshold voltage, V_{th} must be added into Equation (3) to make sure the equation is suitable for real-time system. The new mathematical expression is shown below,

$$V_{LBP}(x_{sa}, y_{sb}) = \begin{cases} (V_{sa} - V_{th}) & ; \quad (x_{sa}, y_{sb}) \text{ inside pipeline} \\ 0 & ; \quad (x_{sa}, y_{sb}) \text{ outside pipeline} \end{cases} \tag{4}$$

Now, the concentration profile that uses Hybrid image reconstruction algorithm can be calculated from the expression below,

$$V_{Hybrid}(x_{sa}, y_{sb}) = \begin{cases} V_{LBP}(x_{sa}, y_{sb}) & ; \quad V_{Sa} \geq V_{th} \text{ AND } V_{Sb} \geq V_{th} \text{ AND } V_{Sc} \geq V_{Sp} \text{ AND } V_{Sd} \geq V_{Sp} \\ 0 & ; \quad V_{Sa} < V_{th} \text{ OR } V_{Sb} < V_{th} \text{ OR } V_{Sc} < V_{Sp} \text{ OR } V_{Sd} < V_{Sp} \end{cases} \tag{5}$$

$$c = a - b + 27 \tag{6}$$

$$d = a + b + 3 \tag{7}$$

where $V_{hybrid}(x_{sa}, y_{sb})$ is voltage of pixel (x_{sa}, y_{sb}) inside the concentration profile that using Hybrid image reconstruction algorithm, V_{Sa} or V_{Sb} is voltage value referring to the sensor S_a or S_b in two orthogonal projections (also called the 16×16 layer), V_{Sc} or V_{Sd} is voltage value referring to the sensor S_c or S_d in two rectilinear projections (also called the 23×23 layer), a is sensor number in between 0 to 15 in 16×16 layer, b is sensor number in between 16 to 31 in 16×16 layer, c is sensor number in between 0 to 22 in 23×23 layer, d is sensor number in between 23 to 45 in 23×23 layer, V_{th} is threshold voltage of 16×16 layer and V_{sp} is threshold voltage of 23×23 layer.

From Equation (5), four conditions are used to verify whether the object appears at the corresponding pixel. As mentioned before, each pixel was crossed by 4 projections beams. If these 4 projections beams in all corresponding sensors output voltage are more than the threshold voltage of each, the corresponding pixel represents the object appears. Equations (6) and (7) are used to determine the position of two receivers on 23×23 layer. Figure 8 shows the four conditions. We assume that both 16×16 layer and 23×23 layer are in one layer.

The concentration profile unit is volt. However, it can be converted into unit of mm^2 by multiplying it with a reference area map as shown in Figure 9. The mathematical expression is as follows,

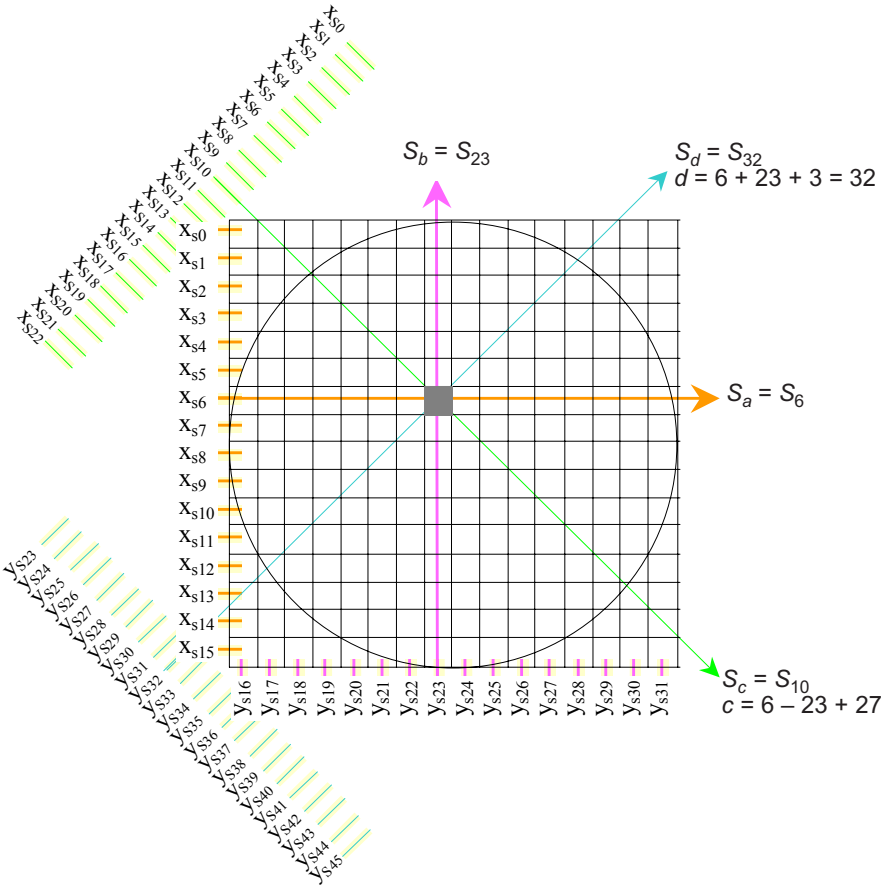

Figure 8 Four corresponding sensors of pixel (x_{S6}, y_{S23})

$$A(x_{sa}, y_{sb}) = \frac{V_{Hybrid}(x_{sa}, y_{sb})}{2(V_m - V_{th})} \times A_{ref}(x_{sa}, y_{sb}) \tag{8}$$

where $A(x_{sa}, y_{sb})$ is area of object in pixel (x_{sa}, y_{sb}) in concentration profile, V_m is maximum sensor output voltage (5 volt), V_{th} is threshold voltage of 16×16 layer and $A_{ref}(x_{sa}, y_{sb})$ is area of pixel (x_{sa}, y_{sb}) within pipeline in reference area map.

The reference area map is determined based on the inner area of the pipeline used in this project. Summing up all pixels area of the map, the answer is equivalent to 5674.5 mm^2 (from $\pi * 42.5^2$) as calculated using formula πr^2.

Since the concentration profile is in the unit of mm^2 already, the cross-sectional area of flow materials can be measured by summing up all pixels' values inside concentration profile as shown in the following equation.

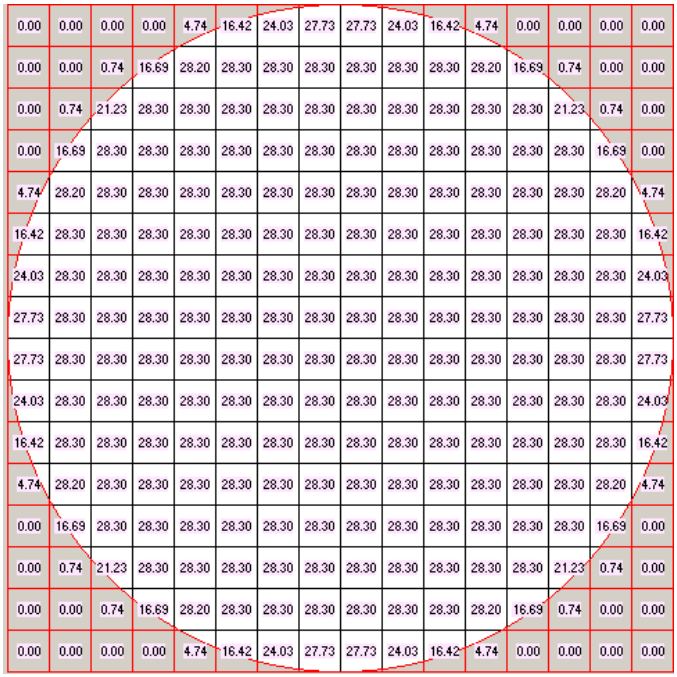

Figure 9 Reference area map

$$A_c = \sum_{a=0}^{15} \sum_{b=16}^{31} A(x_{sa}, y_{sb}) \tag{9}$$

where A_c is measured cross-sectional area.

5.0 RESULTS & DISCUSSIONS

The concentration profile of an object can be predicted by applying the sensor voltage modeling and hybrid image reconstruction algorithm. By multiplying the concentration profile by a specific area map, the cross-sectional area of an object in sensor can be determined easily. Eleven flow pattern models are used to predict their concentration profiles in unit of mm^2 and the calculate their areas. The results obtained will be compared with the real area and the measured area of the corresponding flow model. Besides the single pixel, two pixels and multiple pixels flow pattern models, others are in square, circle, triangular, trapezoid, quarter circle, pentagon, hexagon and oval pattern. They will be tested in two different positions.

Within the table, the actual area of each flow pattern is obtained from the cross-section area of the corresponding model to be used whereas the predicted area of each flow pattern is obtained from the modelling and image reconstruction algorithm. The percentage error of actual-predicted is calculated by using Equation (10) whereas

Table 1 Results of area measurement in various flow models

Flow pattern model	Position	Area (mm^2)			% Error	
		Actual	Predicted	Measured	Actual-predicted	Predicted-measured
Single pixel	–	28.30	28.30	28.30	0.00	0.00
Two pixels	–	56.60	56.60	56.60	0.00	0.00
Multiple pixel	–	84.90	84.90	84.90	0.00	0.00
Square	1	841.00	707.50	707.50	15.87	0.00
	2	841.00	943.33	956.35	–12.17	–1.38
Circle	1	1017.87	905.60	905.60	11.03	0.00
	2	1017.87	1018.80	1018.99	–0.09	–0.02
Triangular	1	659.10	999.93	1000.88	–51.71	–0.10
	2	659.10	955.91	983.52	–45.03	–2.89
Trapezoid	1	797.50	921.32	920.44	–15.53	0.10
	2	797.50	1100.56	1105.27	–38.00	–0.43
Quarter circle	1	907.92	933.90	933.90	–2.86	0.00
	2	907.92	971.63	972.77	–7.02	–0.12
Pentagon	1	871.88	905.60	905.60	–3.87	0.00
	2	871.88	962.20	961.45	–10.36	0.08
Hexagon	1	937.65	993.64	980.19	–5.97	1.35
	2	937.65	1169.73	1165.87	–24.75	0.33
Oval	1	1130.00	1188.60	1185.42	–5.18	0.27
	2	1130.00	1251.49	1254.73	–10.75	–0.26

the percentage error of predicted-measured is computed by using Equation (11). The negative sign of the actual-predicted error obtained shows that the actual area is less than the predicted area. In the same definition, the negative sign of the predicted-measured error obtained shows that the predicted area is less than the measured area.

$$\%\ \text{Error}_{(\text{actual}-\text{predicted})} = \frac{\text{actual area} - \text{predicted area}}{\text{actual area}} \times 100\% \tag{10}$$

$$\%\ \text{Error}_{(\text{predicted}-\text{measured})} = \frac{\text{predicted area} - \text{measured area}}{\text{predicted area}} \times 100\% \tag{11}$$

When plotting the actual, predicted and measured areas into graph, it looks like Figure 10.

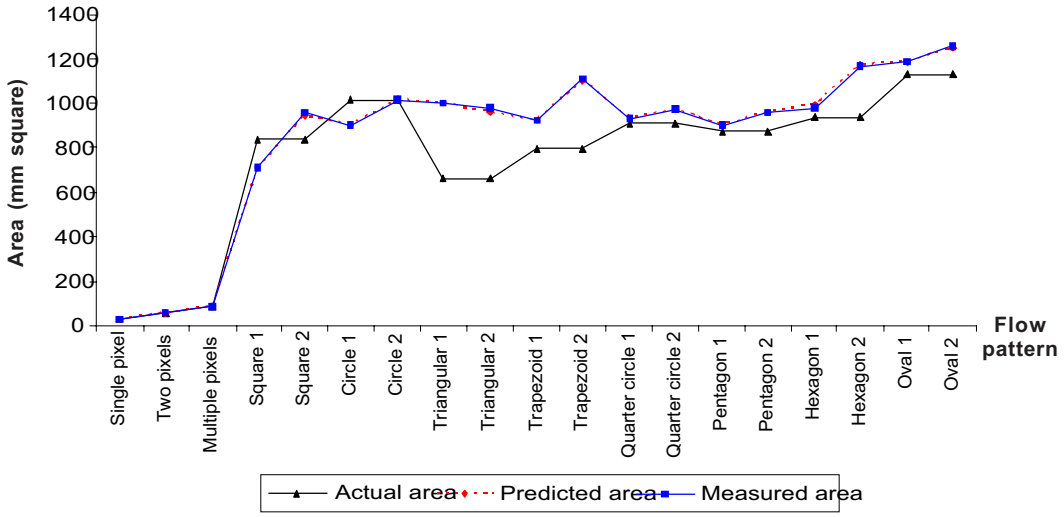

Figure 10 Comparison among actual, predicted and measured area using various flow patterns

From Figure 10, the flow models of single pixel, two pixels and multiple pixels have the same actual area, predicted area and measured area because they are designed ideally. The other flow pattern models can be imagined as the flow patterns of solid particles material in vertical pneumatic conveyor practically. The errors calculated between the flow patterns of actual area versus modelled area and modelled area versus measured area are shown in Figure 11.

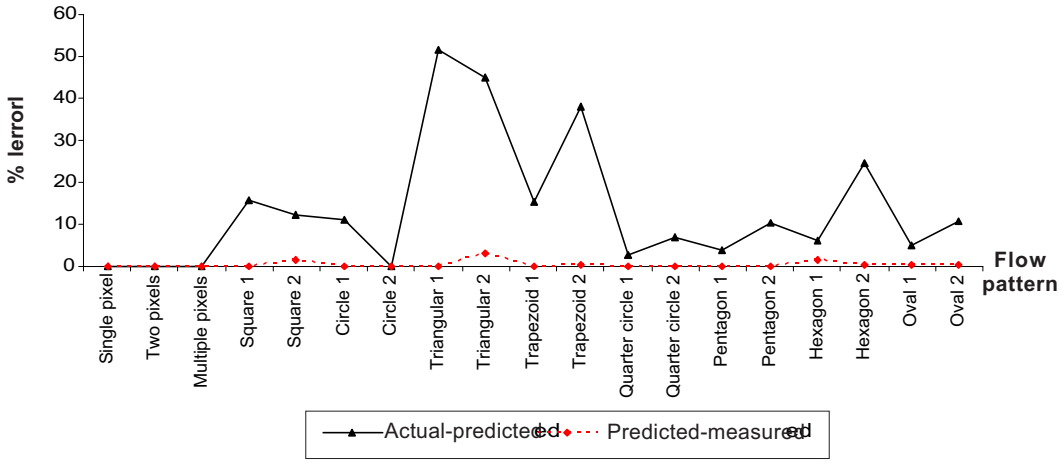

Figure 11 The line graph of percentage error of area measurement

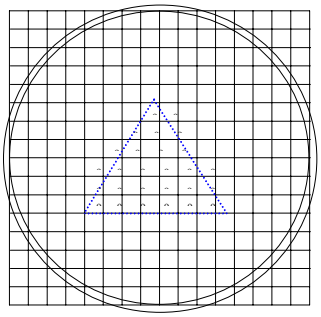

Predicted concentration

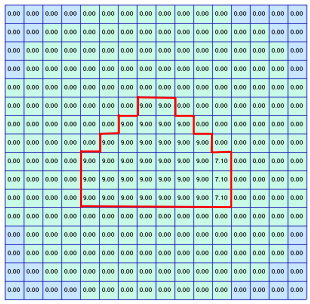

Measured concentration

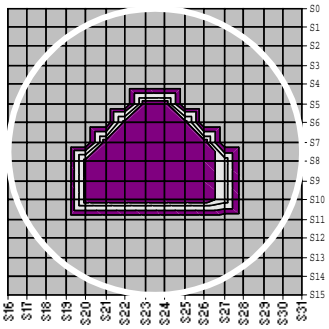

2D and 3D Image

Actual area

Pixel detected

Area
- Actual = 659.10
- Predicted = 999.93 — % error =
- Measured = 1000.88 — % error = 0.10

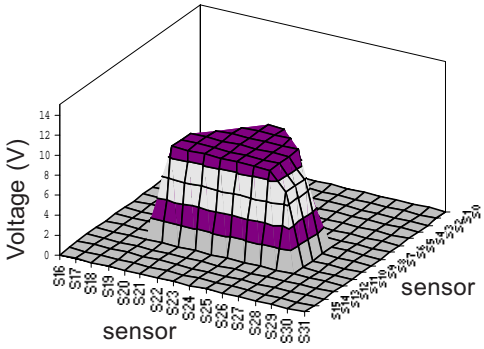

(a) Triangular flow pattern (Position 1)

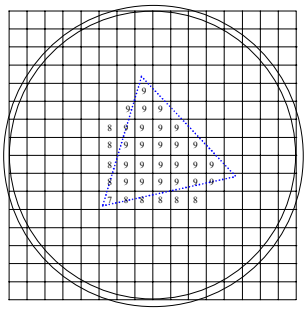

Predicted concentration

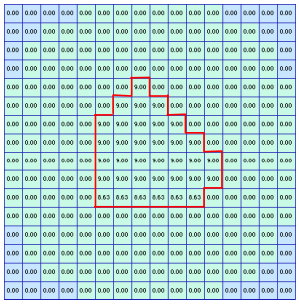

Measured concentration

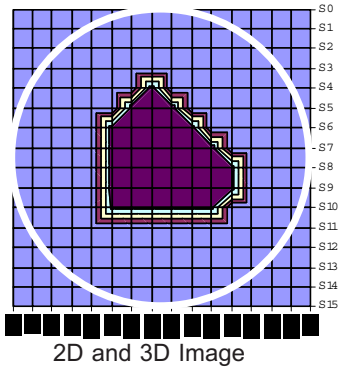

2D and 3D Image

Actual area

Pixel detected

Area
- Actual = 659.10 mm^2
- Predicted = 955.91 mm^2 — % error = 45.03
- Measured = 983.52 mm^2 — % error = 2.89

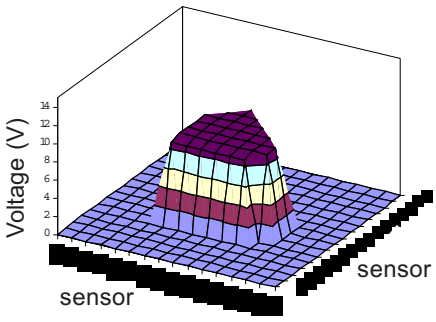

(b) Triangular flow pattern (Position 2)

Figure 12 Concentration measurement of triangular and circle flow patterns

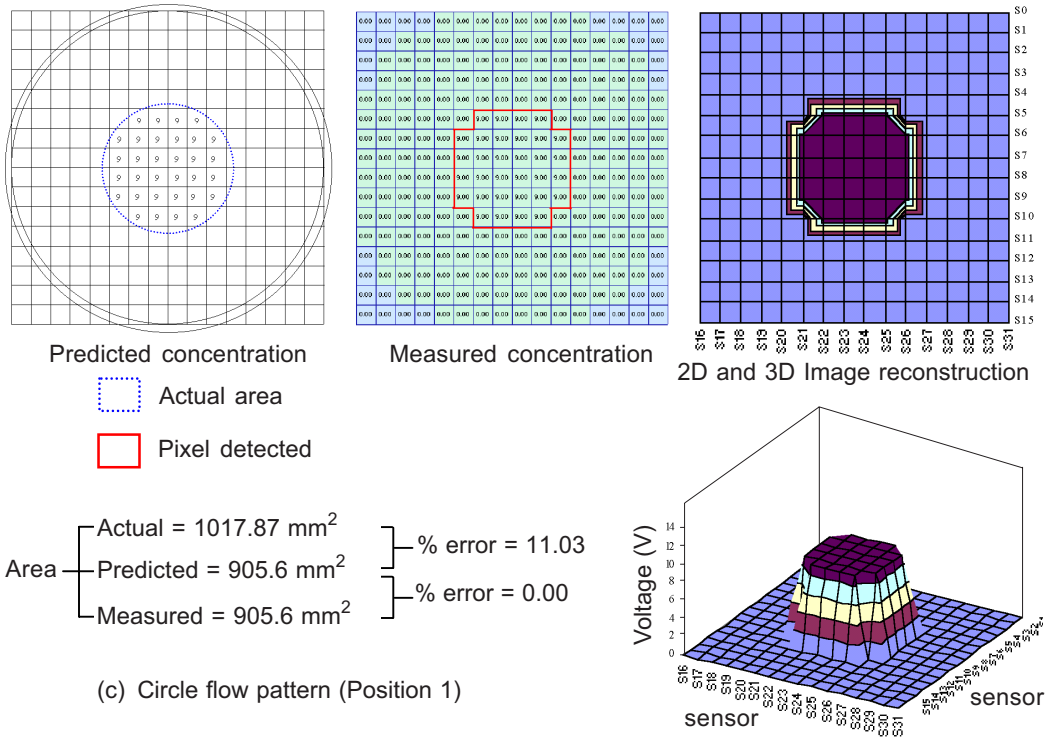

(c) Circle flow pattern (Position 1)

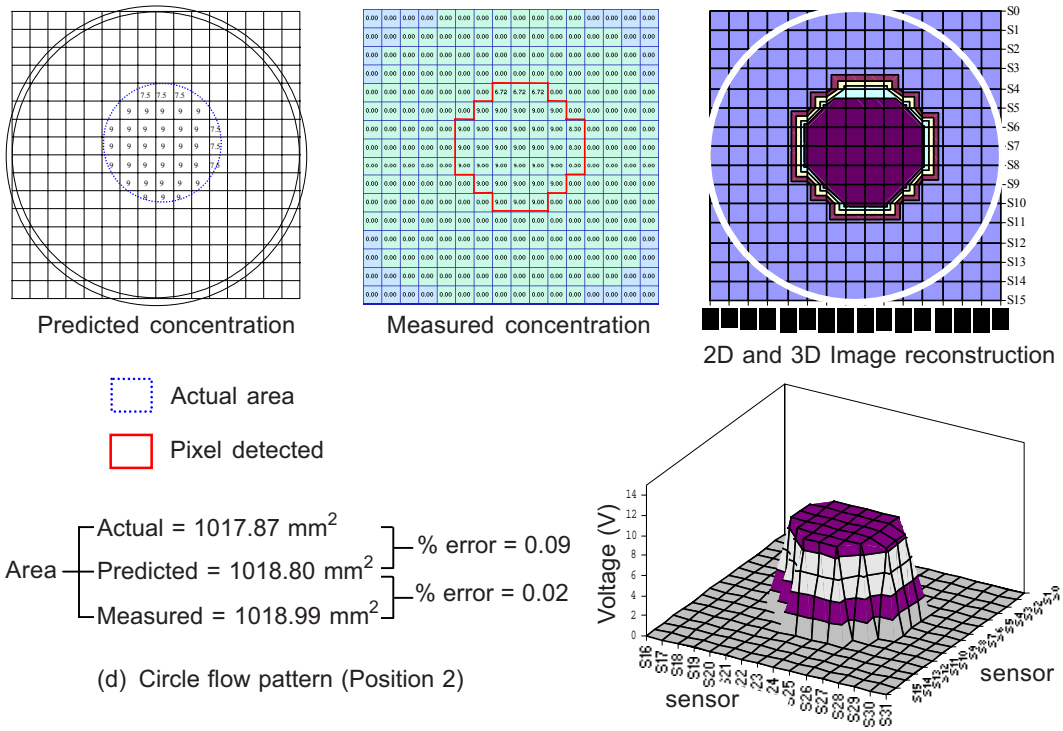

(d) Circle flow pattern (Position 2)

Figure 12 Concentration measurement of triangular and circle flow patterns

The overall error of predicted-measured flow concentration is between 0% to 3% (except for triangular which is consider as illegal flow patterns). It means that the measured results are almost the same as the modelling results. The small error obtained is due to the hardware noise. The triangular flow model has the maximum percentage of error whereas the circular model has the smallest error in both position 1 and position 2. All corresponding concentration profiles in these two cases are shown in Figure 12.

In the comparison of flow concentration between actual area and predicted area, the triangular flow model has the largest error of more than 45% either in position 1 or position 2. All of the flow models that contain curve in boundary have the error less than 12%, such as circle, quarter circle and oval model. The circular model can even achieve 0.09% error of its second position. The error can be reduced by increasing the resolution of the tomography sensor.

6.0 CONCLUSIONS

Concentration measurement has been carried out by using 11 types of flow pattern models. The measurement concentrates on the area of flow model detected. The percentage error between predicted area and measured area is less than 3% in all cases. Besides, investigation on the illegal flow patterns has been described. Empirically, neither parallel beam projections nor fan beam projections can measure the flow pattern that contain 'L', 'U' and 'V' shapes. These kinds of geometries are not selected as the flow models in this project. It can be investigated by referring Figure 13 that shows how fan beam projections are used to detect the flow patterns above according to the fan beam sensor conducted by Chan (2002). The results obtained show that the flow patterns detected contain ambiguous effect. Thus, these kinds of geometries are not selected as the flow models in this project. As a result, all of the flow patterns that being mentioned are considered as the illegal flow patterns and have to be avoided in the flow designation.

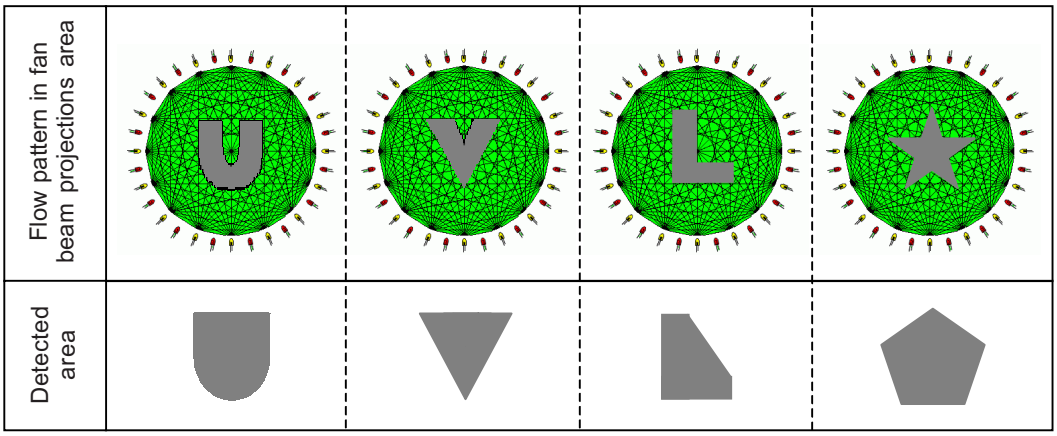

Figure 13 Illegal flow patterns to be detected in optical tomography

It can be concluded that solid particles used in the solid-gas measurement should have the flow pattern of circle or contain curve in flow pattern boundary so that the measured cross-sectional area is closer to the real one.

REFERENCES

[1] William, R. A., and M. S. Beck. 1995. *Process Tomography-Principle Techniques and Applications*. Great-Britain: Butterworth-Heinemann. 3-12.

[2] Abdul Rahim, R. 1996. A Tomography Imaging System for Pneumatic Conveyors Using Optical Fibres. Ph.D. Thesis. Sheffield Hallam University.

[3] Ibrahim, S. 2000. Measurement of Gas Bubbles in a Vertical Water Column Using Optical Tomography. Ph.D. Thesis. Sheffield Hallam University.

[4] Ibrahim, S., R. G. Green, K. Dutton, and R. Abdul Rahim. 2000. Modelling to Optimize the Design of Optical Tomography Systems for Process Measurement. Symposium on Process Tomography. Warsaw, Poland .

[5] Chan, K. S. 2002. Real Time Image Reconstruction for Fan Beam Optical Tomography System. M Sc. Thesis. Universiti Teknologi Malaysia.